



Four steps for revealing and adjusting the 3D structure of aptamers in solution by small-angle X-ray scattering and computer simulation

Felix N. Tomilin^{1,2} · Roman Moryachkov^{1,3} · Irina Shchugoreva^{2,3} · Vladimir N. Zabluda¹ · Georgy Peters⁴ · Mikhail Platunov¹ · Vera Spiridonova⁵ · Anastasia Melnichuk⁵ · Anastasia Atrokhova⁵ · Sergey S. Zamay^{1,3} · Sergey G. Ovchinnikov^{1,2} · Galina S. Zamay^{3,6} · Alexey Sokolov^{1,2} · Tatiana N. Zamay^{3,6} · Maxim V. Berezovski⁷ · Anna S. Kichkailo^{3,6}

Received: 11 April 2019 / Revised: 12 July 2019 / Accepted: 22 July 2019 / Published online: 8 August 2019
© Springer-Verlag GmbH Germany, part of Springer Nature 2019

Abstract

Nucleic acid (NA) aptamers bind to their targets with high affinity and selectivity. The three-dimensional (3D) structures of aptamers play a major role in these non-covalent interactions. Here, we use a four-step approach to determine a true 3D structure of aptamers in solution using small-angle X-ray scattering (SAXS) and molecular structure restoration (MSR). The approach consists of (i) acquiring SAXS experimental data of an aptamer in solution, (ii) building a spatial distribution of the molecule's electron density using SAXS results, (iii) constructing a 3D model of the aptamer from its nucleotide primary sequence and secondary structure, and (iv) comparing and refining the modeled 3D structures with the experimental SAXS model. In the proof-of-principle we analyzed the 3D structure of RE31 aptamer to thrombin in a native free state at different temperatures and validated it by circular dichroism (CD). The resulting 3D structure of RE31 has the most energetically favorable conformation and the same elements such as a B-form duplex, non-complementary region, and two G-quartets which were previously reported by X-ray diffraction (XRD) from a single crystal. More broadly, this study demonstrates the complementary approach for constructing and adjusting the 3D structures of aptamers, DNazymes, and ribozymes in solution, and could supply new opportunities for developing functional nucleic acids.

Keywords Aptamer · Thrombin · Three-dimensional structure · Small-angle X-ray scattering · Molecular modeling

Abbreviations

CD	Circular dichroism	FRET	Fluorescence resonance energy transfer
Cryo-EM	Cryogenic electron microscopy	MSR	Molecular structure restoration
		NMR	Nuclear magnetic resonance spectroscopy

Electronic supplementary material The online version of this article (<https://doi.org/10.1007/s00216-019-02045-0>) contains supplementary material, which is available to authorized users.

✉ Maxim V. Berezovski
maxim.berezovski@uottawa.ca

✉ Anna S. Kichkailo
annazamay@yandex.ru

¹ Kirensky Institute of Physics, Federal Research Center KSC Siberian Branch Russian Academy of Sciences, 50/38 Akademgorodok, Krasnoyarsk 660036, Russia

² Siberian Federal University, 79 Svobodny pr., Krasnoyarsk 660041, Russia

³ Federal Research Center “Krasnoyarsk Science Center” Siberian Branch of the Russian Academy of Sciences, 50 Akademgorodok, Krasnoyarsk 660036, Russia

⁴ NRC Kurchatov Institute, 1, Academic Kurchatov Square, Moscow 123182, Russia

⁵ A.N. Belozersky Institute of Physico-Chemical Biology, Lomonosov Moscow State University, 1/40 Leninskie Gory, Moscow 119992, Russia

⁶ Krasnoyarsk State Medical University, 1 Partizana Zheleznyaka, Krasnoyarsk 660022, Russia

⁷ Department of Chemistry and Biomolecular Sciences, University of Ottawa, 10 Marie-Curie, Ottawa, Ontario K1N6N5, Canada

SAXS Small-angle X-ray scattering
XRD X-ray diffraction

Introduction

Aptamers are synthetic RNA or DNA oligonucleotide ligands capable of recognizing other molecules and may even exhibit catalytic activity. Aptamer–target interactions depend on the aptamer’s three-dimensional (3D) structure, distribution of their charges, and the nature of its binding partner. Various structural elements, such as hairpins, bulges, pseudoknots, and G-quadruplexes [1], ensure aptamer interactions with their targets through hydrogen bonds, hydrophobic interactions, van der Waals interactions, and aromatic stacking [2]. Aptamers are used in a large variety of biosensors [3–9] and therapeutics [6, 10–12]. Aptamer binding depends on its 3D structure. The problem now is that the aptamer’s 3D structure cannot be directly extrapolated from its nucleotide sequence or its secondary structure. To understand the molecular basis of the complex formation, knowledge about a main aptamer spatial conformation is very desirable, but is often unavailable because of limitations of analytical methods for structure analysis. To date, the most common methods to study nucleic acid structures include X-ray diffraction (XRD) [13], nuclear magnetic resonance spectroscopy (NMR) [14–19], small-angle X-ray scattering (SAXS) [20, 21], circular dichroism (CD) [22], fluorescence resonance energy transfer (FRET) [23], and cryogenic electron microscopy (Cryo-EM, mostly for DNA–origami or protein–NA complexes) [24, 25].

The most precise method is XRD crystallographic analysis [26, 27]. However, this method only provides a static picture of one oligonucleotide conformation in the solid state whereas NMR, SAXS, FRET, and CD can probe dynamic conformational changes in solution under more physiologically relevant conditions. NMR finds aptamer conformations in solution with atomic resolution, but this technique is generally limited to small biomolecules (< 30–40 kDa). Alternatively, FRET can only measure the relative distance between fluorescently labeled nucleotides and does not show the structure of a whole molecule [28]. In addition the fluorescent labeling of a nucleic acid may affect its 3D structure. CD spectroscopy is ideal for tracing conformational transitions between discrete nucleic acids motifs (G-quadruplexes, A, B, Z-forms, etc.) [29]. CD is used as a complementary method to NMR spectroscopy and SAXS, because it does not require any labeling [22]. Cryo-EM still has the lowest limit in determination of molecular mass (about > 60 kDa) [30].

SAXS is a powerful technique for structure determination of biomolecules in solution as well as their higher-order assemblies, if the initial constituents are known [20, 21, 31]. The theoretical basis of structural analysis by small-angle scattering on particles was first presented by Guinier [32] and

applied to nucleic acids by Timasheff in 1961 [33]. Small-angle scattering intensity from a particle drops exponentially with an angle, and the index of power is associated with a generalized particle size and its radius of gyration. The magnitude of gyration radius depends on the distribution of the scattering center in space, particle size, and shape. Moreover, the form of the scattered radiation intensity curve with an increasing angle is significantly different for the three basic conformations of biological macromolecules: a ball, stick, and disk. SAXS has several advantages over the other structural techniques including minimal sample preparation time, analyzing individual macromolecules or their complexes in solutions at physiological conditions or at any required temperature, pH, and buffer, and rapid data collection and processing [31]. In our work, we applied four steps for finding and adjusting a 3D structure of a thrombin binding aptamer (RE31) in solution based on molecular modeling according to its nucleotide sequence and SAXS experiments (Fig. 1).

Material and methods

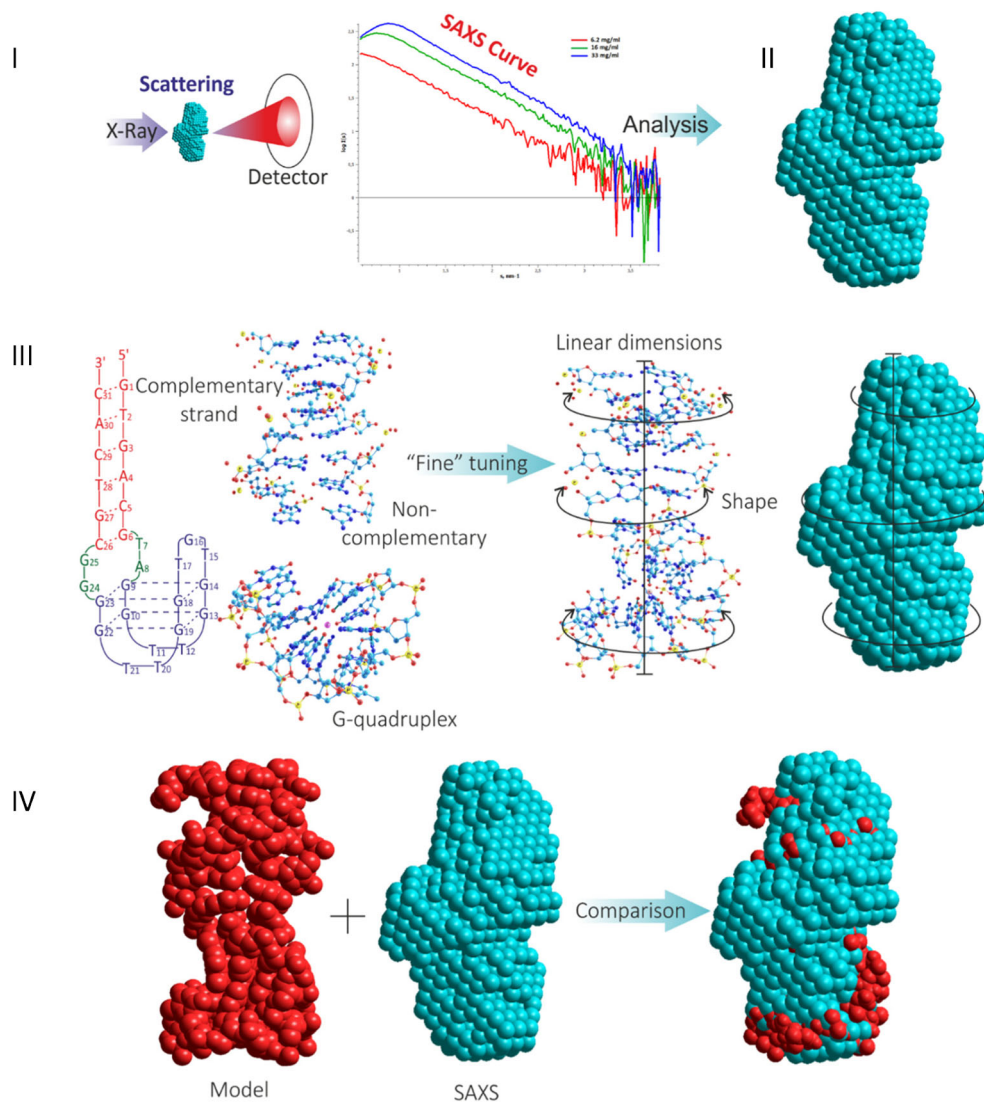
Circular dichroic spectrum analysis and UV-melting

All experiments were performed using inorganic salts and reagents of chemically pure grades (Khimmed, Moscow, Russia). The aptamer RE31 (5'-GTG ACG TAG GTT GGT GTG GTT GGG GCG TCA C-3') was synthesized by the phosphoramidite method by Syntol company (Moscow, Russia). The aptamer was diluted to 2 μM in 20 mM Tris-HCl buffer (pH 7.4) with 5 mM potassium chloride. This solution was heated for 5 min at 90 $^{\circ}\text{C}$, then slowly cooled down, and stored at 20 $^{\circ}\text{C}$ overnight in order to induce folding. The correct folding of the aptamer was verified by recording CD spectra and UV-melting. CD spectra were recorded in the range from 240 to 360 nm in a 1-cm cuvette using a spectrometer (Chirascan, Applied Photophysics Ltd, UK) equipped with a thermoelectric controller. UV spectra were recorded in a 10-mm 400- μl quartz cuvette (Hellma, Germany) using a two-beam U-2900 UV/visible spectrophotometer (Hitachi, Japan).

Small-angle X-ray scattering

RE31 samples (300 μl) in Tris-HCl buffer (pH 7.4) at concentrations of 33, 16, and 6.2 mg ml^{-1} were consecutively placed in a 5-cm-long, 2-mm-diameter, cylindrical capillary and used for SAXS. X-ray synchrotron radiation scattering data was collected at the DICSY station (Kurchatov synchrotron radiation source) at an incident radiation energy of 7.65 keV ($\lambda = 1.62 \text{ \AA}$) using a DECTRIS Pilatus 1M detector (beam size of $0.6 \times 0.4 \text{ mm}$). Instrument calibration was performed just before the experiments using a silver behenate sample with

Fig. 1 General scheme of finding 3D structure of an aptamer with SAXS and molecular structure restoration (MSR). **(I)** acquiring SAXS experimental data of an aptamer in solution, **(II)** building a spatial distribution of the molecule electron density using SAXS results, **(III)** constructing a 3D model of the aptamer from its nucleotide primary sequence and secondary structure, and **(IV)** comparing and refining the modeled 3D structures with the experimental SAXS model (red color, from molecular modeling; blue color, from SAXS data)



an exposure of 60 s. The sample-to-detector distance was 300 mm that provided a scattering vector range from 0.03 to 3.5 nm⁻¹. The data were normalized to the intensity of the transmitted beam and radially averaged. The scattering of the blank solvent was subtracted and the SAXS curve for the DNA aptamer was combined from two concentrations using the PRIMUS program of the ATSAS software suite [34].

Molecular structure restoration

The molecular modeling of RE31 aptamer was carried out according to the sequence, on the basis of SAXS experimental data using the Avogadro program. The resulting atomic structure in all three projections was compared with the experimental model obtained from small-angle scattering [35]. Geometry of the aptamer structure was optimized by a semi-empirical quantum chemical method based on MOPAC2016 [36].

Accession numbers

The coordinates of the structure have been deposited in the Protein Data Bank (Code 3QLP).

Results and discussion

First step: SAXS experimental results

Dependencies of X-ray scattering intensities $I(s)$ on the scattering angle were plotted as shown in Fig. 2. The peaks at low angles of SAXS curve (Fig. 2, $s = 0.5$ – 1.25 nm⁻¹) at 16 and 33 mg ml⁻¹ indicate the presence of interparticle interactions of molecules in solution, i.e., there is interference in molecules that are close to each other. Reduced concentrations of 6.2 mg ml⁻¹ were required. However, measurements at high concentration

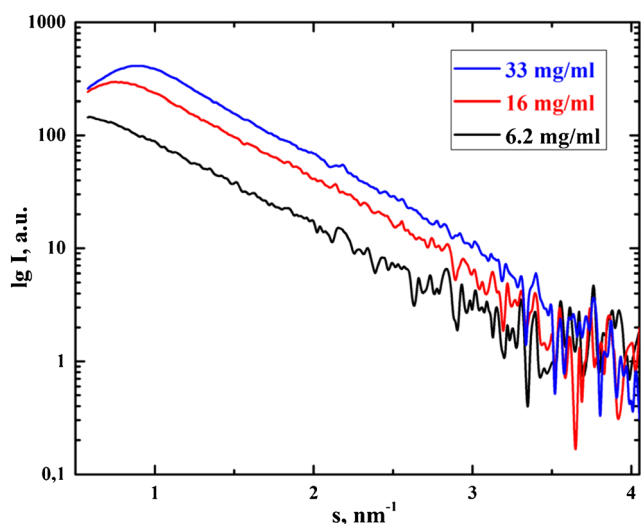


Fig. 2 Dependencies of X-ray intensity on the scattering angle for RE31 aptamer at different concentrations

provided a better signal to noise ratio for the SAXS profile at the high scattering angles. The curve at 6.2 mg ml^{-1} has a good profile at low angles and delivers useful and correct information about the size and overall shape of the molecules (Fig. 3a).

Second step: SAXS modeling

Guinier analysis allows one to estimate the mass distribution with respect to the center of mass in the molecule. It is the slope of the linear approximation of the dependency of scattered radiation intensity $\ln(I)$ versus s^2 in the range of the

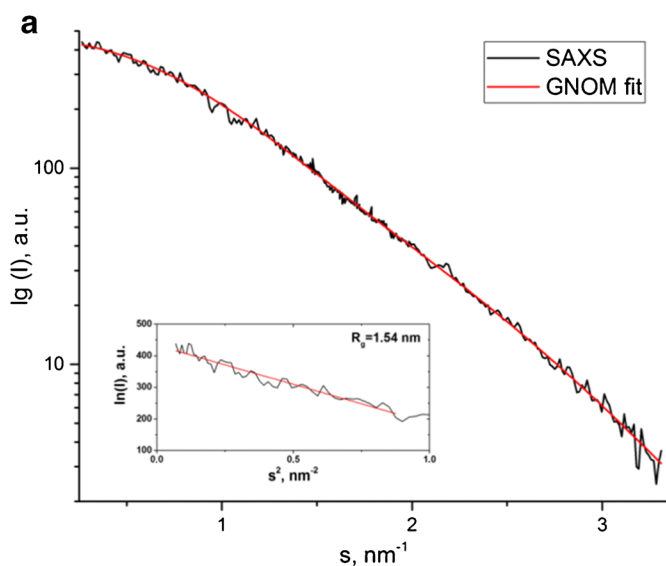


Fig. 3 SAXS fitting. (a) Experimental SAXS data (black) and fitted curve from Gnom program (red) with inserted Guinier plot. The combined SAXS profile includes scattering intensity values at low angles ($0.02 < s < 1.3 \text{ nm}^{-1}$) at the concentration of 6.2 mg ml^{-1} and signal values at high angles ($1.3 < s < 3.3 \text{ nm}^{-1}$) at the concentration of 33 mg ml^{-1} . The Guinier

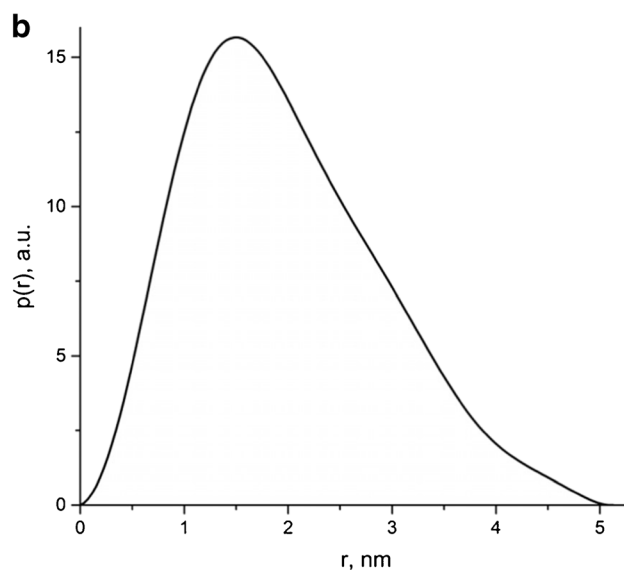
region is defined for approximation as $0.4 < sR_g < 1.3$. Calculated by Guinier approximation, the radius of gyration (R_g) was 1.54 nm .

The distance distribution function $p(r)$ calculated by indirect Fourier transform program GNOM [37] (Fig. 3b) is the SAXS data in real space and displays features of the molecular shape. The function $p(r)$ is defined by the equation

$$p(r) = \frac{r^2}{2\pi^2} \int_0^\infty s^2 I(s) \frac{\sin sr}{sr} ds$$

The value of the $p(r)$ equals zero both at $r = 0$ and $r = D_{\max}$, where D_{\max} is the maximum dimension of the molecule. The distance distribution function has various curve shapes for a ball, disk, and cylinder. The maximum particle diameter (D_{\max}) was defined from $p(r)$ as approximately 5.06 nm .

The RE31 aptamer ab initio structure was constructed in the DAMMIN program [38] in which the molecular structure of the oligonucleotide is represented by densely packed beads placed inside the sphere limited by D_{\max} . Every bead is assigned as “1” corresponding to the molecule electron density or “0” corresponding to the solvent. The software forms a random bead model, calculates the scattering pattern of the model using “simulated annealing”, compares it with experimental data, determines discrepancy, and corrects the model. A low-resolution 3D model of RE31 was obtained using the iterative selection of models and minimization of the goal function by the Monte-Carlo method.



region is defined for approximation as $0.4 < sR_g < 1.3$. (b) Autocorrelation distance distribution function $p(r)$. Maximum r value for the $p(r)$ function is the diameter D_{\max} of the starting spherical volume for ab initio reconstruction

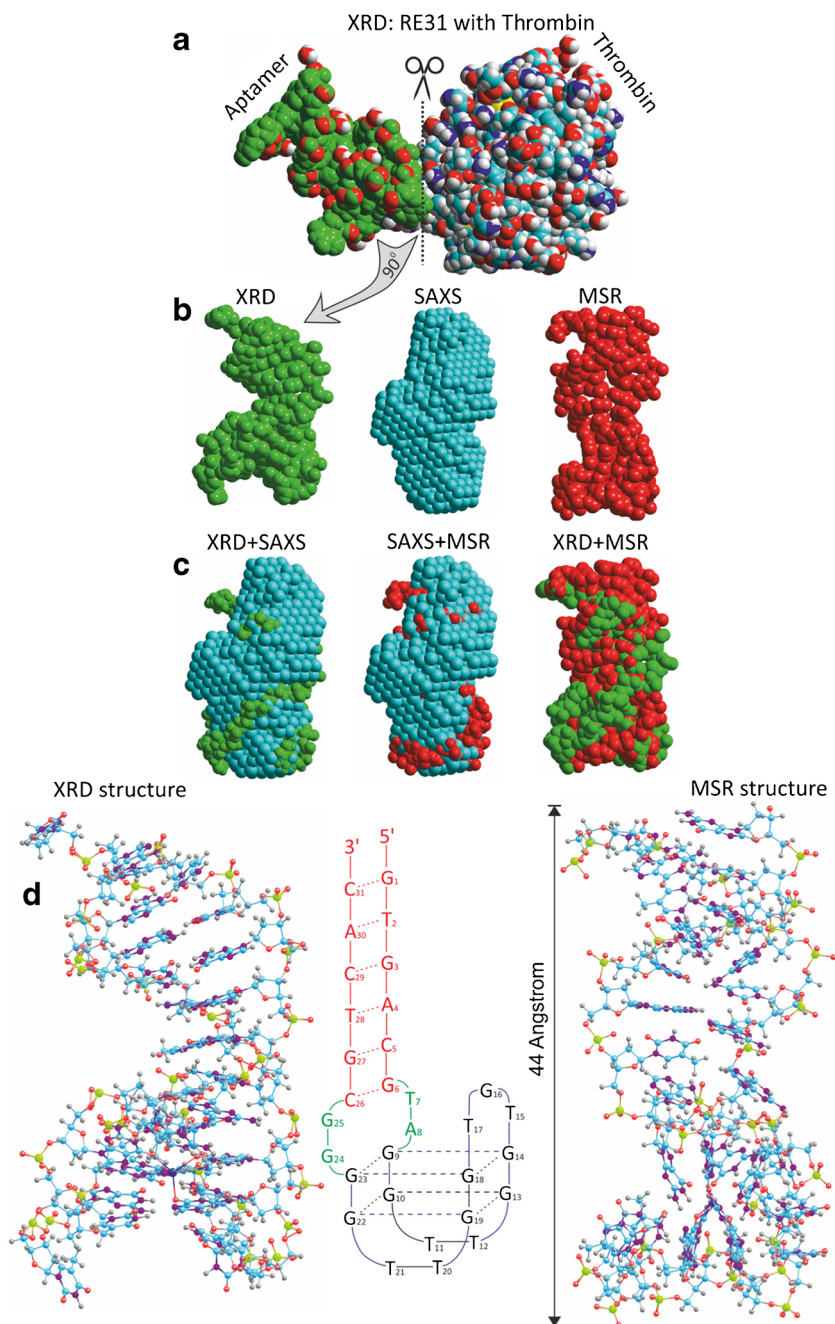
Third step: MSR modeling

The molecular structure restoration modeling of RE31 was carried out with the Avogadro program [39] according to its primary sequence and small-angle scattering experimental data (Fig. 1-II). The primary sequence of RE31 was used to predict the secondary structure by using the Mfold web server [40] on the basis of free energy minimization techniques.

The aptamer was divided into three structural parts and their location in space was varied relative to each other in accordance with experimental data. The first structural part is a G-quadruplex with the following sequence GGTGGGTGTGGTTGG. It is a

well-known 15-nt thrombin binding aptamer (15TBA) formed by two tetrads of four guanines in the classical conformation *anti-syn-anti-syn* and a potassium ion located in the center [41, 42]. The X-ray data of the thrombin complex with 15TBA aptamer has been described previously by the Tulinsky group [43]. The G-quadruplex consists of two stacked planar G-quartets (G-stem) that are associated with three lateral loops. Each G-quartet is connected by eight hydrogen bonds. According to the X-ray data, 15TBA binds to thrombin by embracing the protruding region of exosite I through their TT loops [44, 45]. The second structural part of RE31 is a double-stranded part. This is a right-handed B-type helix. The third structural part consists of four non-

Fig. 4 Comparing RE31 aptamer structures from different methods. (A) RE31–thrombin complex by XRD. (B) Aptamer structures obtained by XRD in green color, SAXS in turquoise color, MSR in red color. (C) Comparison of the structures obtained by different methods. (D) RE31 structures from XRD analysis and MSR. Between them there is RE31 secondary structure divided into the three colored parts; red, a B-form duplex; green, a non-complementary region; blue, a G-quadruplex



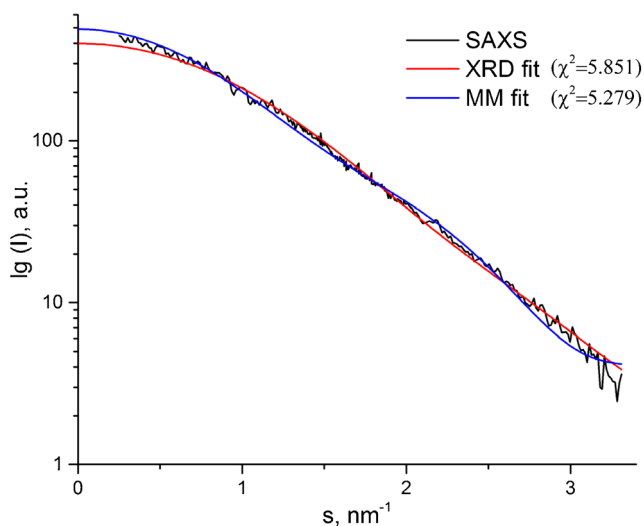


Fig. 5 Fitting SAXS curve with predicted XRD and MSR. The small-angle scattering evaluation was performed in the CRY SOL program. The discrepancy χ^2 between scattering curve from PDB structure and experimental graph is shown in brackets

complementary nucleotides T–G and A–Gs (Fig. 1-III). The dissociation constant of RE31–thrombin complex is 0.16 nM [46].

Fourth step: comparison of SAXS and MSR models

In the fourth step, the molecular modeling was carried out to construct the initial geometry of aptamer molecules in space. The resulting atomic structure was compared with an experimental form obtained from small-angle scattering. At this stage, determining the linear dimensions of molecules in all three projections was the main goal, while it was difficult to achieve a perfect match in the fine details. As DNA is a chiral molecule, different variants of aptamer local twisting are possible. The largest difficulty arises in the molecular design of non-complementary nucleotides, as they have a large number of possible positions. At first, the model with the basic nitrogen atoms turned in different directions was built. However, this structure is not compliant with the experimental volume. In order to make the model fit with the experimental figure, nucleotides making up the double chain were twisted, similar to a double helix. Thus, we achieved the maximum coincidence with the experimental shape. Therefore, in this step, local twisting of nucleotides was carried out to obtain the best possible match with features of the experimental figure (Fig. 1-IV).

The modeled aptamer molecule should match linear dimensions obtained according to the analysis of the SAXS curve. For example, the linear dimensions from SAXS (height 44 Å; width 26, 23, and 25 Å in Fig. 1-III) match well the linear dimensions of the constructed 3D model (44 Å and 23, 20, and 22 Å, respectively) in Fig. 1-III. Furthermore, even on the existing linear

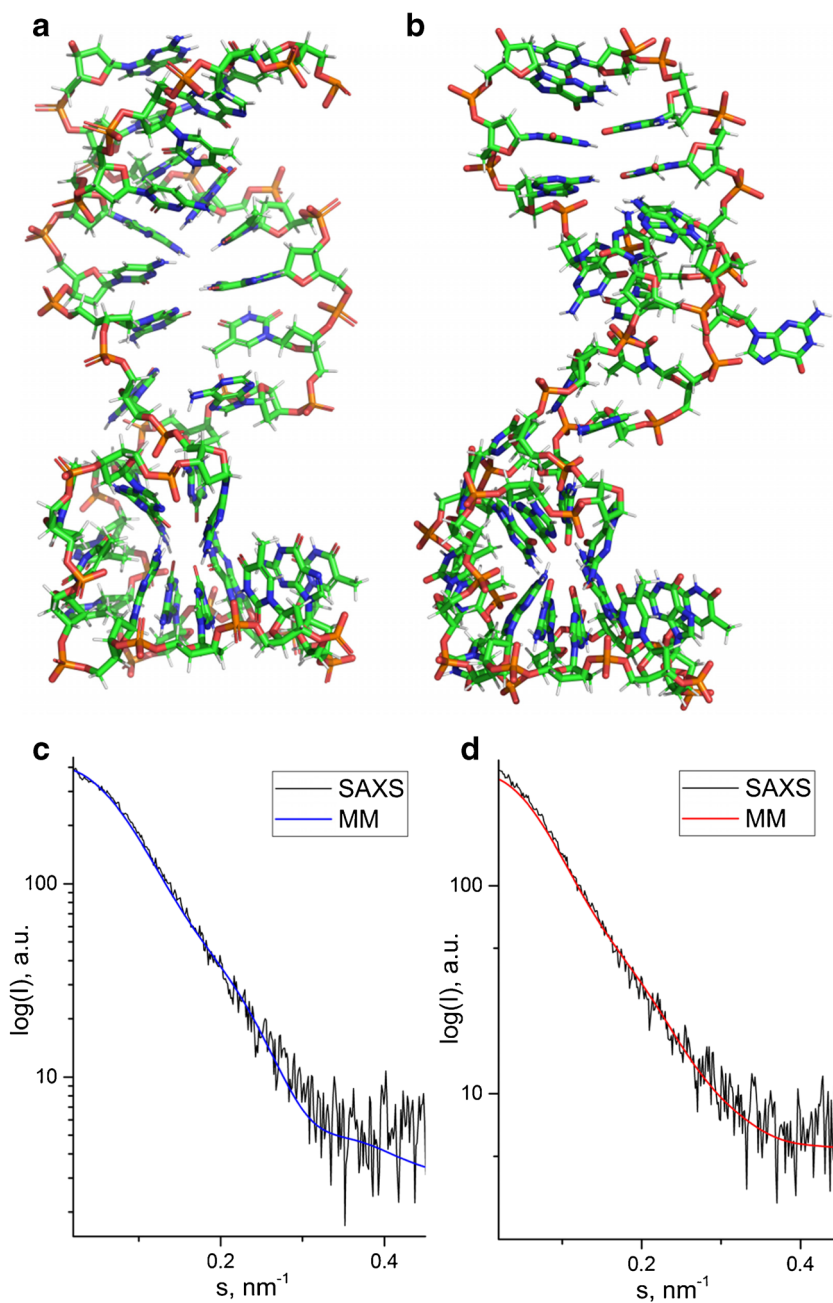
dimensions, it is possible to model a large number of conformations. At the second stage of theoretical modeling it is necessary to ensure that the constructed theoretical model takes into account the peculiarities of the “relief” of the experimentally obtained shape (this shape may have a complex topology). Therefore, in the “fine tuning” step, we achieved (by minor rotations around sigma bonds) the most complete fitting of the theoretical model into the experimental volume. After changing the theoretical geometry of the molecule in accordance with the shape of the electron density from SAXS, we plotted the SAXS curve from the theoretical molecule and compared it with the experimental curve; thus, we checked the consistency of the model with the experiment.

Figure 4 shows the RE31 structure obtained by three different methods. The top image (Fig. 4A) shows the aptamer binding with thrombin revealed by XRD [47]. Figure 4B shows the aptamer structure obtained by XRD, SAXS and MSR. Comparing aptamer conformations obtained by SAXS in solution with XRD from a crystal form with thrombin and MSR showed a good match (Fig. 4C). In both cases, the main difference consists of the quadruplex part of the aptamer, as it acts as a thrombin-binding site. Previously, it was shown that RE31 forms a specific complex with thrombin with an apparent dissociation constant of 0.16 nM [46]. The differences between the aptamer structure before and after addition of the protein can be interpreted as an induced fit model when the aptamer changes its shape upon the binding. Figure 4D shows the RE31 structure constructed from XRD analysis and MSR. The bonding between terminal nucleotides (G1 and C31) is flexible. The duplex part and non-complementary region between the quadruplex and duplex are not static, but rather flexible.

An atomic model in the PDB format can be converted to the SAXS profile and compared with the experimental curve using the CRY SOL program [35]. The program uses spherical harmonic approximation to calculate the scattering pattern from atomic structure factors and Gaussian sphere approximation for each atom’s position in the molecule considering the hydration layer enveloping it. Figure 5 represents the correspondence between the measured SAXS profile and the scattering profiles from XRD and MSR. A discrepancy χ^2 between experimental SAXS curve and evaluated one from the XRD model by the program CRY SOL is 5.851; χ^2 between SAXS and the MSR model is 5.279.

The biggest problem is in molecular modeling of non-complementary nucleotides, as they have a large number of possible positions. The nucleotides are twisted in the double chain, similarly to a double-stranded helix and the resulting model resembles the experimental SAXS results well. Using the SAXS method, we obtained the structure of RE31 in its native free state in Tris-HCl buffer in the presence of monovalent ions without the target protein at room temperature.

Fig. 6 Reconstructed atomic structures and SAXS profiles of the RE31 aptamer at different temperatures. Atomic structures of RE31 at 25 °C (**a**) and 40 °C (**b**). Experimental SAXS and MSR simulated scattering curves at 25 °C (**c**) and 40 °C (**d**)



Testing 3D structure by CD

Prior to SAXS experiments, the structure of RE31 was characterized by CD spectroscopy. The spectrum maximum at 294 nm confirms the presence of the antiparallel G-quadruplex structure in this molecule (see Electronic Supplementary Material (ESM) Fig. S1). Its spectrum changes with an increase in temperature: the maximum intensity at 294 nm decreases, and two isosbestic points at 250 nm and 230 nm are seen, which indicates the transformation of two aptamer conformations (folded to unfolded) during the melting process. The presence of a duplex structure within RE31 (see ESM Fig. S2) was shown using UV-

melting at 260 nm, along with the melting point, which occurred at 37.5 °C. It was shown that the structure of RE31 consisted of a G-quadruplex and duplex domain.

We attempted to predict the conformational changes of the aptamer by molecular modeling of the atomic structure at increasing temperature. Firstly, we recorded the scattering patterns for RE31 at 25 °C and 40 °C and tried to calculate its volume, shape, and size. Then we used these SAXS models in molecular modeling for the conformation refinement. The obtained models for 25 °C and 40 °C are shown in Fig. 6a and b; scattering curves at higher temperatures do not allow one to construct reasonable models. To compare the proximity of the

MSR models to the SAXS, the CRYSOLO fits were created for RE31 at both temperatures (Fig. 6c, d). At 25 °C we can see a good match of experimental SAXS and MSR simulated scattering curves ($\chi^2 = 4.791$). At 40 °C ($\chi^2 = 11.804$) a significant difference at low angles is observed, which can be explained by high mobility of the molecule at this temperature and the growth of the peak similar to the particle repulsion peak.

Testing 3D structure by SAXS at different temperatures

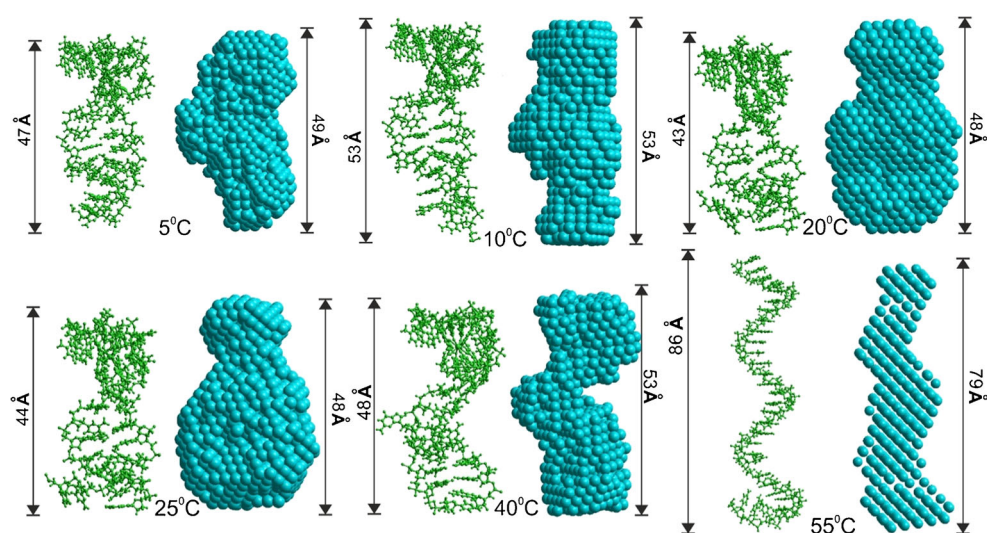
Folding of biomolecules can be qualitatively assessed by a Kratky plot. This representation makes folded and unfolded structures more evident. Characteristic bell-shaped curves at 8 and 25 °C RE31 correspond to a folded structure of RE31 (see ESM Fig. S3b). At 40 °C the peak shifts downward suggesting that the aptamer is only partially folded. When the temperature reaches 50 °C the curve lacks the peak, has a plateau, and increases at larger values representing the unfolded aptamer. When heated, SAXS profiles are compressed at medium angles and increased at low angles (see ESM Fig. S3a). It supports CD data that the melting temperature of the aptamer is 37.5 °C. More MSR and SAXS models at different temperatures are presented at Fig. 7. Scattering curves at temperatures 5–25 °C are almost the same and reconstructed shapes of the RE31 electron density (bead models) have differences quite likely due to the small amount of collected data at high angles. At 40 °C and above there are distinctive conformational changes indicated by SAXS. The differences in the structures are due to the aptamer melting temperature. At 37 °C the aptamer unfolds and elongates, and finally at 55 °C it loses its G-quadruplex structure. The SAXS measurements at higher temperatures demonstrate the open unfolded structure of the aptamer. One of the possible melted RE31 spatial structures is presented in the bottom-right image in Fig. 7.

Conclusions

The purpose of this work is 3D molecular structure restoration of the aptamer from SAXS experiments obtained in solution. The SAXS method gives the shape of a molecule, but not the atomic structure of the aptamer. To solve this problem we used Avogadro software. The building of a molecule uses bond lengths and angles between atoms. In the first approximation, it is reasonable to use the methods of molecular dynamics and/or semi-empirical methods of quantum chemistry, because they allow one to obtain the geometry of the molecule in a reasonable time. Therefore, the PM6 method was used as an auxiliary method for quickly obtaining the bond lengths and angles inside the aptamer molecule. Consequently, neither pH nor other solvent parameters were taken into account (because our purpose is to get a theoretical 3D model according to SAXS experiments).

Nevertheless, there are several limitations for SAXS to be effective. First, a molecule in solution should exist in a single conformation. Therefore, measuring long oligonucleotides (> 150 nt) could be complicated because of interference of multiple structures. Before measuring SAXS, it is better to ensure that the studied molecule forms one configuration with at least 80% probability. To date, several aptamer structures have been obtained using SAXS [27, 33, 47–51]. Thus far the longest aptamer studied by SAXS was the 54-nt aptamer SRB2m and its dimer [42]. Second, SAXS has low resolution around 10 Å that gives only an overall shape of a molecule. This disadvantage could be overcome by using computer simulations of an atomic model based on an aptamer nucleotide sequence and complementary methods such as NMR. The SAXS-based approach finds 3D structure of aptamers in solution without the crystallization required for X-ray diffraction, which may not provide reliable information about the structure in solution of such flexible molecules as nucleic acids. The success of the proposed approach is highly dependent on the knowledge

Fig. 7 Comparison of the MSR and SAXS models at different temperatures



about primary DNA structure. In general, the work described here creates the starting structure for an actual structure determination using NMR restraints and molecular mechanics, but without the energy minimization or water molecules. It may further be applied for finding 3D structures of aptamers, DNazymes, and ribozymes, and could supply new opportunities for developing functional nucleic acids.

Acknowledgements Authors are grateful to Ana Gargaun for English grammar correction. This work was funded in parts by the Ministry of Science and Higher Education of the Russian Federation; project 0287-2019-0007 the Council of the President of the Russian Federation for Support of Young Scientists and Leading Scientific Schools (project no. SP-938.2015.5) and the grant of KSAI “Krasnoyarsk Regional Fund of Supporting Scientific and Technological Activities” for M.P., the internship “The study of the stacking of the secondary structure of DNA aptamers to thrombin” for R.M.

Author contributions V.N. Zabluda, S.S. Zamay, S.G. Ovchinnikov created an idea, designed the overall concept, supervised the work. R. Moryachkov, M. Platonov, G. Peters, V.N. Zabluda, A. Melnichuk performed SAXS experiments, F.N. Tomilin, I. Shchugoreva, S.G. Ovchinnikov, A. Sokolov perform modeling, V. Spiridonova, A. Melnichuk, A. Atrokhova performed circular dichroic spectrum analysis and UV-melting, F.N. Tomilin, S.S. Zamay, G.S. Zamay, T.N. Zamay, M.V. Berezovski, R. Moryachkov, M. Platonov, A.S. Kichkailo analyzed all data and wrote the paper. All authors provided intellectual input, edited and approved the final manuscript.

Compliance with ethical standards

Conflict of interest All authors declare that they have no conflict of interest.

Compliance with ethical standards This article does not contain any studies with human participants or animals performed by any of the authors.

References

- Mascini M, Palchetti I, Tombelli S. Nucleic acid and peptide aptamers: fundamentals and bioanalytical aspects. *Angew Chem Int Ed Engl.* 2012;51(6):1316–32. <https://doi.org/10.1002/anie.201006630>.
- Hermann T, Patel DJ. Adaptive recognition by nucleic acid aptamers. *Science.* 2000;287(5454):820–5. <https://doi.org/10.1126/science.287.5454.820>.
- Labib M, Zamay AS, Kolovskaya OS, Reshetneva IT, Zamay GS, Kibbee RJ, et al. Aptamer-based impedimetric sensor for bacterial typing. *Anal Chem.* 2012;84(19):8114–7. <https://doi.org/10.1021/ac302217u>.
- Labib M, Zamay AS, Kolovskaya OS, Reshetneva IT, Zamay GS, Kibbee RJ, et al. Aptamer-based viability impedimetric sensor for bacteria. *Anal Chem.* 2012;84(21):8966–9. <https://doi.org/10.1021/ac302902s>.
- Liu J, Cao Z, Lu Y. Functional nucleic acid sensors. *Chem Rev.* 2009;109(5):1948–98. <https://doi.org/10.1021/cr030183i>.
- Pang X, Cui C, Wan S, Jiang Y, Zhang L, Xia L, et al. Bioapplications of cell-SELEX-generated aptamers in cancer diagnostics, therapeutics, theranostics and biomarker discovery: a comprehensive review. *Cancers (Basel).* 2018;10(2). <https://doi.org/10.3390/cancers10020047>.
- Zhang J, Liu B, Liu H, Zhang X, Tan W. Aptamer-conjugated gold nanoparticles for bioanalysis. *Nanomedicine (Lond).* 2013;8(6):983–93. <https://doi.org/10.2217/nmm.13.80>.
- Zhou W, Huang PJ, Ding J, Liu J. Aptamer-based biosensors for biomedical diagnostics. *Analyst.* 2014;139(11):2627–40. <https://doi.org/10.1039/c4an00132j>.
- Zimbres FM, Tarnok A, Ulrich H, Wrenger C. Aptamers: novel molecules as diagnostic markers in bacterial and viral infections? *Biomed Res Int.* 2013;2013:731516. <https://doi.org/10.1155/2013/731516>.
- Keefe AD, Pai S, Ellington A. Aptamers as therapeutics. *Nat Rev Drug Discov.* 2010;9(7):537–50. <https://doi.org/10.1038/nrd3141>.
- Kruspe S, Mittelberger F, Szameit K, Hahn U. Aptamers as drug delivery vehicles. *ChemMedChem.* 2014;9(9):1998–2011. <https://doi.org/10.1002/cmdc.201402163>.
- Sun H, Zhu X, Lu PY, Rosato RR, Tan W, Zu Y. Oligonucleotide aptamers: new tools for targeted cancer therapy. *Molecular Ther Nucleic Acids.* 2014;3:e182. <https://doi.org/10.1038/mtna.2014.32>.
- Kennard O, Hunter WN. Oligonucleotide structure: a decade of results from single crystal X-ray diffraction studies. *Q Rev Biophys.* 1989;22(3):327–79.
- Adrian M, Heddi B, Phan AT. NMR spectroscopy of G-quadruplexes. *Methods.* 2012;57(1):11–24. <https://doi.org/10.1016/j.jymeth.2012.05.003>.
- Kyogoku Y. NMR studies on structure and interaction of proteins and nucleic acids in solution. *Tanpakushitsu Kakusan Koso.* 1995;40(3):327–39.
- Mao X, Marky LA, Gmeiner WH. NMR structure of the thrombin-binding DNA aptamer stabilized by Sr²⁺. *J Biomol Struct Dyn.* 2004;22(1):25–33. <https://doi.org/10.1080/07391102.2004.10506977>.
- van Buuren BN, Schleucher J, Wittmann V, Griesinger C, Schwalbe H, Wijmenga SS. NMR spectroscopic determination of the solution structure of a branched nucleic acid from residual dipolar couplings by using isotopically labeled nucleotides. *Angew Chem Int Ed Engl.* 2004;43(2):187–92. <https://doi.org/10.1002/anie.200351632>.
- van der Werf RM, Tessari M, Wijmenga SS. Nucleic acid helix structure determination from NMR proton chemical shifts. *J Biomol NMR.* 2013;56(2):95–112. <https://doi.org/10.1007/s10858-013-9725-y>.
- Leupin W, Wagner G, Denny WA, Wuthrich K. Assignment of the ¹³C nuclear magnetic resonance spectrum of a short DNA-duplex with ¹H-detected two-dimensional heteronuclear correlation spectroscopy. *Nucleic Acids Res.* 1987;15(1):267–75. <https://doi.org/10.1093/nar/15.1.267>.
- Hammel M. Validation of macromolecular flexibility in solution by small-angle x-ray scattering (SAXS). *Eur Biophys J.* 2012;41(10):789–99. <https://doi.org/10.1007/s00249-012-0820-x>.
- Rambo RP, Tainer JA. Super-resolution in solution x-ray scattering and its applications to structural systems biology. *Annu Rev Biophys.* 2013;42:415–41. <https://doi.org/10.1146/annurev-biophys-083012-130301>.
- Vieville JM, Barluenga S, Winsinger N, Delsuc MA. Duplex formation and secondary structure of gamma-PNA observed by NMR and CD. *Biophys Chem.* 2016;210:9–13. <https://doi.org/10.1016/j.bpc.2015.09.002>.
- Preus S, Wilhelmsson LM. Advances in quantitative FRET-based methods for studying nucleic acids. *Chembiochem.* 2012;13(14):1990–2001. <https://doi.org/10.1002/cbic.201200400>.
- Bai XC, Martin TG, Scheres SH, Dietz H. Cryo-EM structure of a 3D DNA-origami object. *Proc Natl Acad Sci U S A.* 2012;109(49):20012–7. <https://doi.org/10.1073/pnas.1215713109>.
- Martin TG, Bharat TA, Joerger AC, Bai XC, Praetorius F, Fersht AR, et al. Design of a molecular support for cryo-EM structure

- determination. *Proc Natl Acad Sci U S A*. 2016;113(47):E7456–E63. <https://doi.org/10.1073/pnas.1612720113>.
26. Nunn CM, Van Meervelt L, Zhang SD, Moore MH, Kennard O. DNA-drug interactions. The crystal structures of d(TGTACA) and d(TGATCA) complexed with daunomycin. *J Mol Biol*. 1991;222(2):167–77.
 27. Ruijgrok VJ, Levisson M, Hekelaar J, Smidt H, Dijkstra BW, van der Oost J. Characterization of aptamer-protein complexes by x-ray crystallography and alternative approaches. *Int J Mol Sci*. 2012;13(8):10537–52. <https://doi.org/10.3390/ijms130810537>.
 28. Bood M, Sarangamath S, Wranne MS, Grotli M, Wilhelmsson LM. Fluorescent nucleobase analogues for base-base FRET in nucleic acids: synthesis, photophysics and applications. *Beilstein J Org Chem*. 2018;14:114–29. <https://doi.org/10.3762/bjoc.14.7>.
 29. Paramasivan S, Rujan I, Bolton PH. Circular dichroism of quadruplex DNAs: applications to structure, cation effects and ligand binding. *Methods*. 2007;43(4):324–31. <https://doi.org/10.1016/j.ymeth.2007.02.009>.
 30. Orlova EV, Saibil HR. Structural analysis of macromolecular assemblies by electron microscopy. *Chem Rev*. 2011;111(12):7710–48. <https://doi.org/10.1021/cr100353t>.
 31. Jeffries CM, Graewert MA, Blanchet CE, Langley DB, Whitten AE, Svergun DI. Preparing monodisperse macromolecular samples for successful biological small-angle x-ray and neutron-scattering experiments. *Nat Protoc*. 2016;11(11):2122–53. <https://doi.org/10.1038/nprot.2016.113>.
 32. Guinier A. L'espriit de la recherche aux U. S. A. *Atomes*. 1947;2(20):378–82.
 33. Timasheff SN, Witz J, Luzzati V. The structure of high molecular weight ribonucleic acid in solution. A smallangle x-ray scattering study. *Biophys J*. 1961;1:525–37.
 34. Petoukhov MV, Franke D, Shkumatov AV, Tria G, Kikhney AG, Gajda M, et al. New developments in the ATSAS program package for small-angle scattering data analysis. *J Appl Crystallogr*. 2012;45(Pt 2):342–50. <https://doi.org/10.1107/S0021889812007662>.
 35. Svergun D, Barberato C, Koch MHJ. CRY SOL - a program to evaluate x-ray solution scattering of biological macromolecules from atomic coordinates. *J Appl Crystallogr*. 1995;28(6):768–73. <https://doi.org/10.1107/S0021889895007047>.
 36. Stewart JJP. MOPAC2016. Stewart Computational Chemistry, Colorado Springs, CO, USA. <http://openmopac.net/MOPAC2016.html>. 2016
 37. Svergun DI. Determination of the regularization parameter in indirect-transform methods using perceptual criteria. *J Appl Crystallogr*. 1992;25(4):495–503. <https://doi.org/10.1107/S0021889892001663>.
 38. Svergun DI. Restoring low resolution structure of biological macromolecules from solution scattering using simulated annealing. *Biophys J*. 1999;76(6):2879–86. [https://doi.org/10.1016/S0006-3495\(99\)77443-6](https://doi.org/10.1016/S0006-3495(99)77443-6).
 39. Hanwell MD, Curtis DE, Lonie DC, Vandermeersch T, Zurek E, Hutchison GR. Avogadro: an advanced semantic chemical editor, visualization, and analysis platform. *J Cheminform*. 2012;4(1):17. <https://doi.org/10.1186/1758-2946-4-17>.
 40. Zuker M. Mfold web server for nucleic acid folding and hybridization prediction. *Nucleic Acids Res*. 2003;31(13):3406–15. <https://doi.org/10.1093/nar/gkg595>.
 41. Ikebukuro K, Okumura Y, Sumikura K, Karube I. A novel method of screening thrombin-inhibiting DNA aptamers using an evolution-mimicking algorithm. *Nucleic Acids Res*. 2005;33(12):e108. <https://doi.org/10.1093/nar/gni108>.
 42. Macaya RF, Waldron JA, Beutel BA, Gao H, Joesten ME, Yang M, et al. Structural and functional characterization of potent antithrombotic oligonucleotides possessing both quadruplex and duplex motifs. *Biochemistry*. 1995;34(13):4478–92.
 43. Padmanabhan K, Tulinsky A. An ambiguous structure of a DNA 15-mer thrombin complex. *Acta Crystallogr D Biol Crystallogr*. 1996;52(Pt 2):272–82. <https://doi.org/10.1107/S0907444995013977>.
 44. Russo Krauss I, Merlino A, Giancola C, Randazzo A, Mazzarella L, Sica F. Thrombin-aptamer recognition: a revealed ambiguity. *Nucleic Acids Res*. 2011;39(17):7858–67. <https://doi.org/10.1093/nar/gkr522>.
 45. Russo Krauss I, Merlino A, Randazzo A, Novellino E, Mazzarella L, Sica F. High-resolution structures of two complexes between thrombin and thrombin-binding aptamer shed light on the role of cations in the aptamer inhibitory activity. *Nucleic Acids Res*. 2012;40(16):8119–28. <https://doi.org/10.1093/nar/gks512>.
 46. Spiridonova VA, Barinova KV, Glinkina KA, Melnichuk AV, Gainutdinov AA, Safenkova IV, et al. A family of DNA aptamers with varied duplex region length that forms complexes with thrombin and prothrombin. *FEBS Lett*. 2015;589(16):2043–9. <https://doi.org/10.1016/j.febslet.2015.06.020>.
 47. Werner A, Konarev PV, Svergun DI, Hahn U. Characterization of a fluorophore binding RNA aptamer by fluorescence correlation spectroscopy and small angle x-ray scattering. *Anal Biochem*. 2009;389(1):52–62. <https://doi.org/10.1016/j.ab.2009.03.018>.
 48. Baird NJ, Ferre-D'Amare AR. Analysis of riboswitch structure and ligand binding using small-angle x-ray scattering (SAXS). *Methods Mol Biol*. 2014;1103:211–25. https://doi.org/10.1007/978-1-62703-730-3_16.
 49. Mittelberger F, Meyer C, Waetzig GH, Zacharias M, Valentini E, Svergun DI, et al. RAID3—an interleukin-6 receptor-binding aptamer with post-selective modification-resistant affinity. *RNA Biol*. 2015;12(9):1043–53. <https://doi.org/10.1080/15476286.2015.1079681>.
 50. Reinstein O, Neves MA, Saad M, Boodram SN, Lombardo S, Beckham SA, et al. Engineering a structure switching mechanism into a steroid-binding aptamer and hydrodynamic analysis of the ligand binding mechanism. *Biochemistry*. 2011;50(43):9368–76. <https://doi.org/10.1021/bi201361v>.
 51. Ruijgrok VJ, van Duijn E, Barendregt A, Dyer K, Tainer JA, Stoltenburg R, et al. Kinetic and stoichiometric characterisation of streptavidin-binding aptamers. *Chembiochem*. 2012;13(6):829–36. <https://doi.org/10.1002/cbic.201100774>.

Publisher's note Springer Nature remains neutral with regard to jurisdictional claims in published maps and institutional affiliations.